ACS APPLIED MATERIALS & INTERFACES

Research Article

www.acsami.org

Carbon Nanoparticle-based Ratiometric Fluorescent Sensor for Detecting Mercury Ions in Aqueous Media and Living Cells

Minhuan Lan,[†] Jinfeng Zhang,[†] Ying-San Chui,[†] Pengfei Wang,*[,‡] Xianfeng Chen,[†] Chun-Sing Lee,[†] Hoi-Lun Kwong,[∥] and Wenjun Zhang*[,†]

[†]Center of Super-Diamond and Advanced Films (COSDAF) and Department of Physics and Materials Science, City University of Hong Kong, Hong Kong SAR, People's Republic of China

[‡]Nano-organic Photoelectronic Laboratory and Key Laboratory of Photochemical Conversion and Optoelectronic Materials, Technical Institute of Physics and Chemistry, Chinese Academy of Sciences, Beijing, 100190, People's Republic of China

[∥]Department of Biology and Chemistry, City University of Hong Kong, Hong Kong SAR, People's Republic of China

S *Supporting Information*

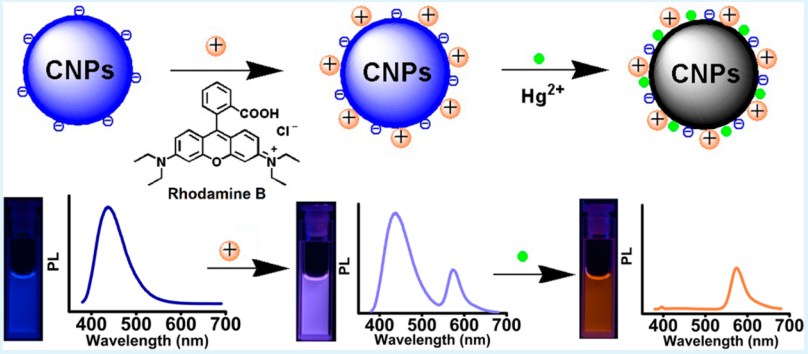

ABSTRACT: A novel nanohybrid ratiometric fluorescence sensor is developed for selective detection of mercuric ions (Hg^{2+}), and the application has been successfully demonstrated in HEPES buffer solution, lake water, and living cells. The sensor comprises water-soluble fluorescent carbon nanoparticles (CNPs) and Rhodamine B (RhB) and exhibits their corresponding dual emissions peaked at 437 and 575 nm, respectively, under a single excitation wavelength (350 nm). The photoluminescence of the CNPs in the nanohybrid system can be completely quenched by Hg^{2+} through effective electron or energy transfer process due to synergetic strong electrostatic interaction and metal−ligand coordination between the surface functional group of CNPs and Hg^{2+}, while that of the RhB remains constant. This results in an obviously distinguishable fluorescence color variation (from violet to orange) of the nanohybrid solution. This novel sensor can effectively identify Hg^{2+} from other metal ions with relatively low background interference even in a complex system such as lake water. The detection limit of this method is as low as 42 nM. Furthermore, the sensing technique is applicable to detect Hg^{2+} in living cells.

KEYWORDS: *ratiometric fluorescence sensor, carbon nanoparticles, bioimaging, mercury ions*

1. INTRODUCTION

Heavy metal ion pollution is a severe problem in environmental protection and human health. Mercury(II) (Hg^{2+}) ions are among the most hazardous and ubiquitous pollutants.[1,2] Hg^{2+} can easily pass through biological membranes and lead to DNA damage, mitosis impairment, and permanent harm to the central nervous system.[3−5] Due to its high toxicity even at a trace concentration, specific and sensitive determination of Hg^{2+} is of particular interest in biological, toxicological, and environmental monitoring. To date, many methods have been established to determine Hg^{2+} concentration, including atomic absorption/emission spectroscopy, inductively coupled plasma mass spectrometry, X-ray absorption spectroscopy, and surface enhanced Raman scattering.[6−11] However, these techniques are either time-consuming or laboratory-based and require expensive instruments. Recently, a variety of fluorescent sensors have been widely used in complex biological samples analysis, as they are well-known for their simplicity, rapid response, and capacity of real-time and in situ monitoring of the dynamic biological processes in living cells.[12−17] Various fluorescent probes including organic molecules[18−22] and semiconductor quantum dots[23−25] show great potential in sensitive detection of Hg^{2+}. However, these fluorescent probes often suffer from complex synthesis routes or involve toxic or expensive reagents, which hinders their practical applications.

To address these problems, photoluminescent carbon nanoparticles (CNPs) are an ideal candidate and have been receiving growing interest. Compared with semiconductor

Received: September 12, 2014
Accepted: November 13, 2014
Published: November 13, 2014

Scheme 1. Dual-Emission Fluorescence Sensing of Hg^{2+} Based on a CNP−RhB Nanohybrid System

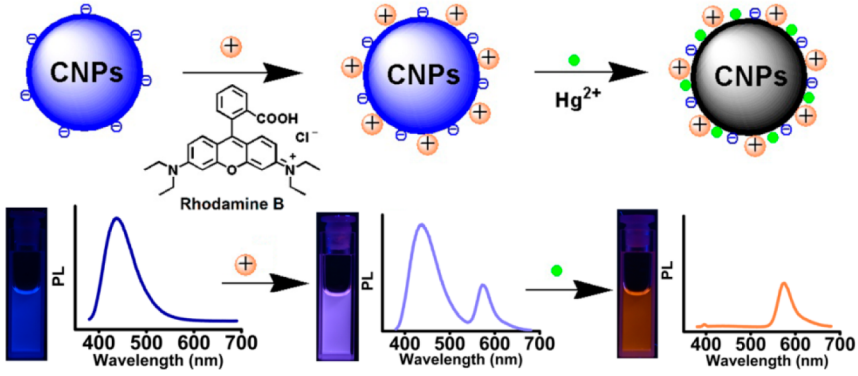

quantum dots, CNPs possess outstanding properties including chemical inertness, excellent photostability, favorable biocompatibility, low toxicity, good water solubility, and cheap cost.[26−29] CNPs have been applied in bioimaging and biosensing,[30−34] including probing Hg^{2+} in aqueous solutions. For example, Goncçalves et al. reported a Hg^{2+} sensor based on functionalized CNPs obtained by laser ablation; the fluorescence intensity of CNPs could be quenched by about 25% and 13% in the presence of 2.7 μM Hg^{2+} and 2.7 μM Cu^{2+}, respectively.[35] Zhou et al. prepared CNPs by pyrolysis of ethylenediaminetetraacetic acid (EDTA) salts at 400 °C and observed that their fluorescence decreased from 11.0% to 8.9% after addition of 40 μM Hg^{2+} in a basic solution (pH 8.5) within 5 min.[36] Lu et al. presented the use of pomelo peel to synthesize CNPs with a fluorescence quantum yield of 6.9% and reported that their photoluminescence (PL) intensity at 444 nm could be quenched by about 60% at 16 min after the addition of 40 μM Hg^{2+}.[37] Very recently, Yan et al. synthesized two kinds of CNPs using citric acid and different nitrogen sources. The fluorescence intensity of these CNPs could be quenched 80 and 55% upon the addition of 20 μM Hg^{2+}.[38]

Overall, these CNP-based sensors adopt fluorescence quenching as the signal output, but the reported approaches are not ready for practical use. The problems include: (1) the fluorescence quantum yield of CNPs is generally low and the quenching is only 80% or well below at very high concentrations of Hg^{2+}; (2) the sensor has a sole emission peak, so during sensing, only the intensity changes while the color remains the same. With these issues, the sensor change needs to be monitored by instruments, and it is not achievable to observe the sensing by naked eyes. Furthermore, the change of single emission peak intensity can be easily affected by a variety of factors such as instrumental efficiency, environmental conditions and external quenchers.[39] To address this limitation, we have developed a ratiometric fluorescence strategy. Such a system is often composed of two individual materials with different fluorescence emission wavelengths. In sensing, the different emissions have different responses to analytes. For example, one emission peak can be severely quenched, while the other one is constant. Therefore, the sensor can clearly change color during sensing, which can be easily recognized. In the meantime, by comparing the variation of the ratio of the two fluorescence intensities before and after sensing, the background interferences could be effectively eliminated and the sensitivity of the sensor could be improved, so they have become a powerful tool for the detection of trace amounts of analytes.[40−42]

Making use of this concept, herein, we report a novel ratiometric fluorescence sensor containing CNPs and Rhodamine B (RhB; Scheme 1) for reliable, selective, and sensitive sensing of Hg^{2+} in a wide pH range and in the interference of other coexisting metal ions. The sensor is built through the electrostatic attraction between negatively charged CNPs and positively charged RhB molecules. This nanohybrid system possesses dual emission peaks at 437 and 575 nm under a single wavelength excitation of 350 nm. The addition of Hg^{2+} to CNP−RhB nanohybrid solution results in rapid and complete fluorescence quenching of CNPs, while the orange fluorescence of RhB keeps constant. During sensing, the fluorescence of CNP−RhB nanohybrid solution gradually changes from violet to orange with the addition of Hg^{2+}. This can be conveniently observed by the naked eyes under UV irradiation. Furthermore, the CNP−RhB nanohybrid system shows high selectivity toward Hg^{2+} over other competing metal ions and amino acids. By taking advantage of the observed PL change, we can fabricate a facile ratiometric fluorescence sensor that allows differentiate of Hg^{2+} from other metal ions in a real sample (lake water) and in living cells.

2. EXPERIMENTAL SECTION

2.1. Materials and Measurements. Rhodamine B, melamine, trisodium citrate dihydrate, *N*-Ethylmaleimide (NEM), NaCl, KCl, $Mn(OAc)_2$-$4H_2O$, $Co(OAc)_2$, $Ni(OAc)_2$, $Al(NO_3)_3$-$9H_2O$, $Cu(OAc)_2$-H_2O, $FeCl_3$, $Cs(OAc)_2$-H_2O, $CeCl_3$-$7H_2O$, $LiNO_3$, $Ba(OAc)_2$, $MgCl_2$-$6H_2O$, $CdSO_4$, $Zn(NO_3)_2$-$6H_2O$, $Pb(NO_3)_2$, $HgCl_2$, HEPES, RNA, DNA, cysteine (Cys), homocysteine (Hcy), glutathione (GSH), serine (Ser), valine (Val), tyrosine (Tyr), leucine (Leu), tryptophan (Trp), alanine (Ala), aspartic acid (Asp), methionine (Met), threonine (Thr), isoleucine (Ile), glycine (Gly), argine (Arg), and lysine (Lys) were purchased from Sigma-Aldrich Co., LLC. All chemicals were used as received without further purification. Deionized water with conductivity of 18.2 MΩ cm^{-1} used in this experiment was purified through a Millipore water purification system. The UV−vis spectra and PL spectra were obtained with Shimadzu 1700 spectrophotometer and Horiba Fluormax-4 spectrophotometer, respectively, at room temperature. The pH measurements were carried out on a Mettler Toledo Delta 320 pH meter.

2.2. Preparation and Characterizations of Fluorescent CNPs. CNPs were prepared by microwave-assisted hydrothermal treatment of melamine and trisodium citrate dihydrate. The detailed synthesis procedures and characterizations were reported in our previous report.[43] X-ray photoelectron spectroscopy (XPS) analysis was measured on a VG ESCALAB 220i-XL surface analysis system. X-ray diffraction (XRD) pattern was obtained using an X-ray diffractometer (Bruker, D2 PHASER). Fourier transform infrared spectroscopy (FTIR) was performed on an IFS 66 V/S (Bruker) IR spectrometer in the range of 400−4000 cm^{-1}. Transmission electron

microscopy (TEM) was performed on a Philips CM200 electron microscope. Zeta potential was recorded on Zetasizer 3000 HS (Malvern, UK).

2.3. Absorption and Fluorescence Assay of Hg^{2+}. The detection of Hg^{2+} was performed in HEPES buffer solution (10 mM, pH 7.2) at room temperature. In a typical run, 100 μL of CNPs dispersion solution (0.2 mg/mL) was added into 1.9 mL HEPES buffer solution in the presence of 1 μM RhB, followed by the addition of calculated amount of Hg^{2+}. The sensitivity and selectivity measurements were conducted in triplicate.

2.4. Cell Culture and in Vitro Imaging Studies. A549 cells were obtained from the Peking Union Medical College. They were cultured in culture medium (DMEM/F12 supplemented with 10% FBS, 50 unit/mL penicillin, and 50 μg/mL of streptomycin) at 37 °C in a humidified incubator containing 5% CO_2. For cell imaging studies, cells were seeded in a 96-well plate at a density of 10^4 cells per well in culture medium and maintained at 37 °C in a 5% CO_2/95% air incubator for 24 h. Then, the cells were incubated with 200 μL CNP−RhB nanohybrid solution in culture medium for 4 h at 37 °C and then washed by PBS twice. These cells were imaged using Nikon fluorescence microscopy (excitation light source: 330−380).

To evaluate the sensing ability to Hg^{2+}, we pretreated A549 cells with 4 mM NEM for 1 h to reduce the concentration of thiol-containing biomolecules and then incubated them with 200 μL of CNP−RhB aqueous solution in culture medium for another 4 h at 37 °C. After the medium was removed and the cells were carefully washed with PBS twice, we then incubated the cells with 20 μM Hg^{2+} aqueous solution for another 5 min at 37 °C. Fluorescence images of living A549 cells were obtained by NIKON fluorescence microscopy.

2.5. MTT Assay. A549 cells were seeded in a 96-well plate at a density of 10^4 cells per well in culture medium and maintained at 37 °C in a 5% CO_2/95% air incubator for 24 h. Then, the culture medium was removed, and the cells were incubated in culture medium containing the as-prepared CNPs or CNP−RhB nanohybrid solution with different concentrations (CNPs: 0, 0.06, 0.12, 0.25, 0.5, 1.0 mg/mL. CNP−RhB nanohybrid system: 0−0; 0.06 mg/mL, 1.5 μM; 0.12 mg/mL, 3.0 μM; 0.25 mg/mL, 6.0 μM; 0.5 mg/mL, 12 μM; 1 mg/mL, 25 μM) for 24 h and washed with culture medium. Then, 200 μL of the new culture medium (without FBS) containing MTT (3-(4,5-dimethylthiazol-2-yl)-2,5-diphenyltetrazolium bromide, 20 μL, 5 mg/mL) was added, followed by incubation for another 4 h to allow the formation of formazan crystals. Absorbance was measured at 570 nm. Cell viability values were determined (five times) according to the following formula: cell viability (%) = (the absorbance of experimental group/the absorbance of blank control group) ×100.

3. RESULTS AND DISCUSSION

To build up our designed sensor, we first prepared CNPs by a simple microwave-assisted hydrothermal method using melamine and trisodium citrate dihydrate as the precursors. Figure 1 shows the TEM image of CNPs, revealing that the nanoparticles have a diameter ranging from 15 to 20 nm. X-ray photoelectron spectroscopy (XPS; Figure S1, Supporting Information) and FT-IR spectra (Figure S2, Supporting Information) reveal that the CNPs mainly contain carbon, nitrogen, oxygen, and the surfaces of the CNPs are functionalized with amino, hydroxyl, and carboxylic/carbonyl moieties. The zeta-potential of CNPs aqueous solution is −56.7 mV (Figure S3, Supporting Information). The fluorescence quantum yield is about 31.5%, which is higher than most of reported CNPs. Remarkably, the fluorescence properties of these CNPs show good stability under high-salt conditions (1 M NaCl) and in a wide pH range (pH 5−13; Figure S4, Supporting Information).

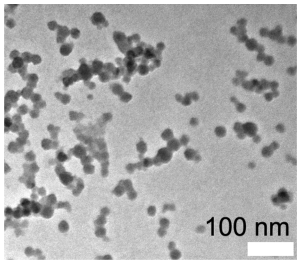

Figure 1. TEM image of as-prepared CNPs.

RhB was selected as the reference signal for built-in calibration in the sensor due to its chemical inertness in the presence of Hg^{2+}. Figure 2a presents the emission spectra of RhB upon addition of Hg^{2+}. It is clear that the PL spectra remain almost unchanged upon the addition of Hg^{2+} up to a concentration of 12 μM. In contrast, the PL of CNPs dramatically decreases in the presence of very low concentration of Hg^{2+} and is completely quenched when the concentration of Hg^{2+} goes up to 10 μM. The fluorescence quenching of CNPs by Hg^{2+} is presumably due to nonradiative electron/hole annihilation through effective electron or energy transfer process, which resulted from the strong electrostatic interaction and metal−ligand coordination between CNPs and Hg^{2+}[36,37] (Figure 2a,b). Based on these findings, we expect that the PL of CNPs in the hybrid sensor can be selectively quenched by Hg^{2+} with high sensitivity, while that of RhB remains unchanged in the sensing process.

Prior to sensor preparation, the interaction between CNPs and RhB in the hybrid system was first investigated by monitoring their absorption and fluorescence spectra changes. As shown in Figure 2c, the maximum absorption peak of CNPs and RhB are at about 342 and 554 nm, respectively, but for RhB, weak absorbance can also be observed in the wavelength range from around 330 to 370 nm. Therefore, it is possible to select a 350 nm wavelength laser to excite both materials in the hybrid sensor. Under 350 nm excitation, the nanohybrid system exhibits two well-resolved emission peaks at 437 and 575 nm. Notably, we can find that there is a narrow overlap between the absorption spectrum of RhB and the PL spectrum of CNPs. However, in the overlap range, the PL of CNPs is rather weak. Therefore, the energy transfer is trivial. This can be confirmed by the results shown in Figure S5 (Supporting Information). Upon the addition of RhB, the CNPs' fluorescence only displays very little decrease.

To obtain a ratiometric fluorescence sensor with an appropriate color variation during sensing, we prepared a mixture solution containing CNPs (100 μL) and RhB (1 μM) as the probe solution for Hg^{2+} detection.

The interaction between CNP−RhB nanohybrid and Hg^{2+} in HEPES buffer solution (10 mM, pH 7.2) was studied by absorption and PL spectroscopy. As shown in Figure 3a, the UV−vis spectrum of CNP−RhB nanohybrid solution displays characteristic absorption bands of CNPs and RhB. Upon addition of Hg^{2+} to the nanohybrid solution, the absorbance at about 352 nm decreases, and a new peak at 308 nm is observed; meanwhile, the absorbance at 554 nm drops monotonically. To further understand the variation of UV−vis spectra in Figure 3a, we studied separately the absorption spectra of CNPs and RhB in the absence and presence of Hg^{2+}. As shown in Figure S6 (Supporting Information), upon the addition of Hg^{2+}, the absorption peak of CNPs at 342 nm is blue-shifted to 318 nm, while the absorption peak of RhB at 554 nm shows trivial change. Based on these observations, we believe that the variation of the UV−vis spectra of CNP−RhB nanohybrid

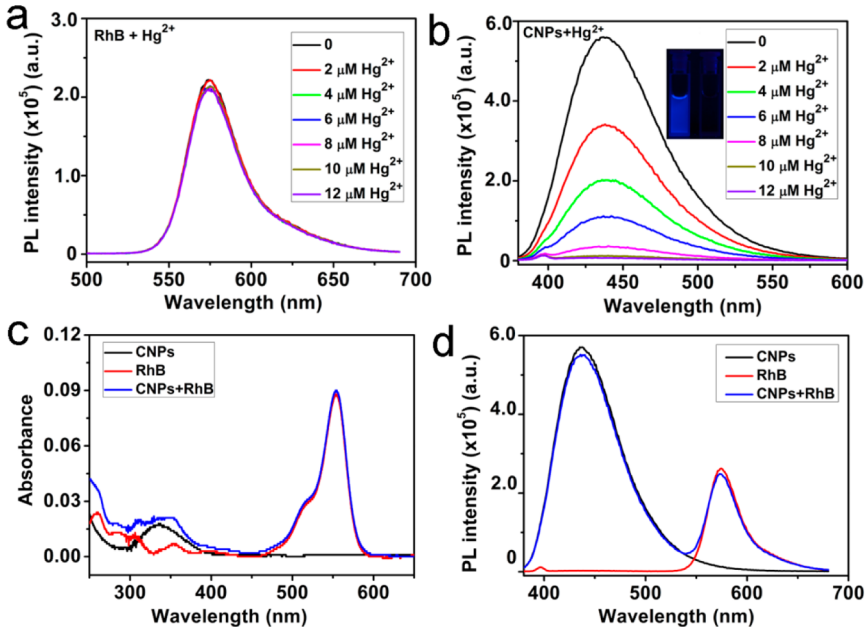

Figure 2. Fluorescence titration spectra of (a) RhB and (b) CNPs in HEPES buffer solution (10 mM, pH 7.2) upon gradual addition of Hg^{2+} from 0 to 12 μM. (λ_{ex} = 350 nm); (b, inset) photograph of CNP solution in the (left) absence and (right) presence of 12 μM Hg^{2+} under a UV light (365 nm). (c) Absorption and (d) PL spectra of (black line) CNPs, (red line) RhB, and (blue line) CNP−RhB nanohybrid solutions.

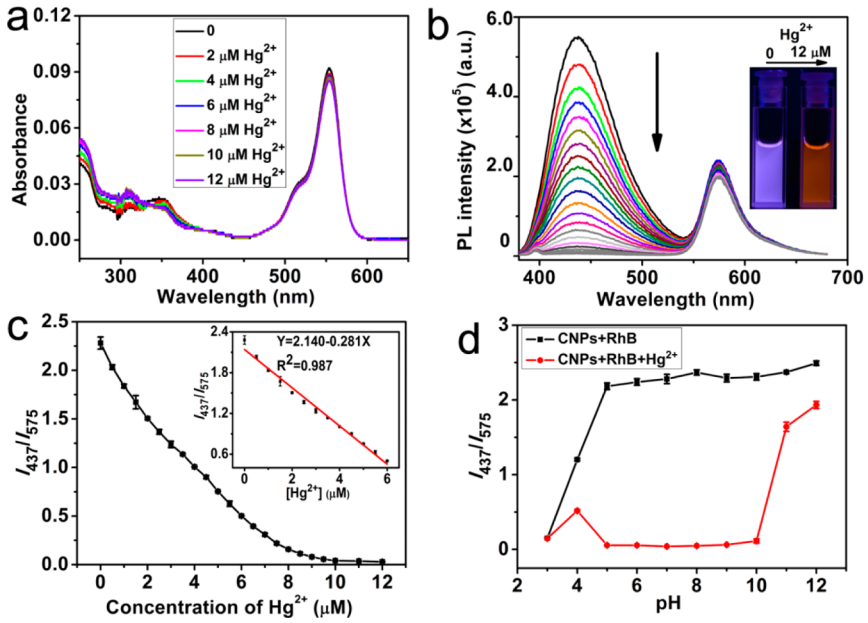

Figure 3. (a) Absorption and (b) fluorescence titration spectra of CNP−RhB nanohybrid system in HEPES buffer solution (10 mM, pH 7.2) upon gradual addition of Hg^{2+} from 0 to 12 μM. (λ_{ex} = 350 nm); (b, inset) photograph of CNP−RhB nanohybrid solution in the (left) absence and (right) presence of 12 μM Hg^{2+} under a UV light (365 nm). (c) The PL intensity ratio (I_{437}/I_{575}) of CNP−RhB nanohybrid solution versus the concentration of Hg^{2+} (0−12 μM); (inset) graph showing the linear relations between I_{437}/I_{575} and the concentrations of Hg^{2+} from 0 to 6 μM. (d) Effect of pHs on the I_{437}/I_{575} ratio of CNP−RhB nanohybrid solution in the (black line) absence and (red line) presence of 12 μM Hg^{2+} at room temperature. All values were obtained based on three independent measurements.

solution upon addition of Hg^{2+} may be attributed to the interaction between CNPs and Hg^{2+}. Their corresponding changes in the fluorescence spectra are shown in Figure 3b. In the absence of Hg^{2+}, CNP−RhB nanohybrid solution shows two emission peaks at 437 and 575 nm. Upon increasing the concentration of Hg^{2+}, the intensity of blue emission from the CNPs continuously and dramatically decreases, while the PL of RhB shows only little drop. Based on these results, it is obvious the CNP−RhB nanohybrid system can rationally detect Hg^{2+} in HEPES buffer solution (10 mM, pH 7.2) through a ratiometric fluorescence approach. The changes of the PL intensity lead to an easily distinguishable fluorescence color of the CNP−RhB nanohybrid solution with change from violet to orange (Figure 3b, inset). The advantages of the ratiometric fluorescence probe for visual detection can be demonstrated by the comparison with the single fluorescence quenching probe of CNPs (Figure 2b, inset), which can be easily affected by sample concentrations and UV light intensity. The corresponding effect can be

dx.doi.org/10.1021/am5062568 | ACS Appl. Mater. Interfaces 2014, 6, 21270−21278

quantitatively evaluated by analyzing the dependence of the PL intensity ratio (I_{437}/I_{575}) on the concentration of Hg^{2+}. As shown in Figure 3c, the I_{437}/I_{575} ratio gradually reduces with the increase of the concentration of Hg^{2+}, and saturates at $[Hg^{2+}]$ of 10 μM. Further addition of Hg^{2+} does not induce detectable changes in the PL spectra. By plotting the I_{437}/I_{575} ratio versus the concentrations of Hg^{2+}, we obtain a good linear relationship (I_{437}/I_{575} = 2.14−0.28 × $[Hg^{2+}]$, R^2 = 0.987) for the Hg^{2+} concentration ranging from 0 to 6 μM (Figure 3c, inset). On this basis, the detection limit, defined as 3 times the standard deviation of background, was calculated to be 42 nM.[44−46] Recently, Liu et al. reported an ultrasensitive fluorescent sensor based on carbon dots, the sensing system achieved a limit of detection as low as 1 fM.[47] According to the United States Environmental Protection Agency, the maximum contaminant level of mercury is 0.002 mg/L (2 ppb, 10 nM) in drinking water.[48] The sensitivity of our system needs to be further improved for application in water detection. We can further improve the quantum yield of the CNPs and tailor the surface to have high affinity with Hg^{2+} to enhance the sensitivity of the sensor.

To further study the practical applicability of this sensor, we investigated the effects of pH on the PL response to Hg^{2+} of CNP−RhB nanohybrid system. Experimental results show that the I_{437}/I_{575} ratio of CNP−RhB nanohybrid solution is relatively constant in a wide pH range of 5−12 (Figure 3d, black line) in the absence of Hg^{2+}. Upon addition of 12 μM Hg^{2+}, the PL of CNPs is completely quenched and therefore the I_{437}/I_{575} ratio significantly diminishes (Figure 3d, red line) and remains a low value of close to 0 between pH 5 and 10. This reveals that the CNP−RhB nanohybrid system can be used to probe Hg^{2+} in a wide pH range of 5 to 10. Under strong acidic conditions (pH < 5), the carboxyl and amino groups on the surface of CNPs may be partially protonated, which decrease the electrostatic interaction of sensor and Hg^{2+}. On the other hand, at pH of greater than 10, Hg^{2+} and OH^- may form $Hg(OH)_2$ complex, which also weakens the electrostatic interaction of sensor and Hg^{2+} and thus reduces the sensitivity.

Besides sensitivity, selectivity is another important parameter to evaluate the performance of a sensing system. The specificity of the CNP−RhB nanohybrid system for Hg^{2+} with a variety of environmentally relevant metal ions including Li^+, Na^+, K^+, Mg^{2+}, Ba^{2+}, Mn^{2+}, Co^{2+}, Cu^{2+}, Cd^{2+}, Cs^{2+}, Ni^{2+}, Zn^{2+}, Pb^{2+}, Fe^{3+}, Al^{3+} and Ce^{3+} was evaluated in HEPES buffer solution (10 mM, pH 7.2). We first investigated whether these metals alone can quench the sensor platform. As illustrated in Figure 4a, the I_{437}/I_{575} ratio is nearly unchanged in the presence of other metal ions (Figure 4a, black columns). However, the addition of Hg^{2+} can completely quench the PL of CNP solution, even when it coexists with large amounts of other types of metal ions, and result in significant diminishing of I_{437}/I_{575} ratio (Figure 4a, red columns). This finding indicates that our sensing system exhibits a high specificity for Hg^{2+} against other metal ions. Such an outstanding selectivity and specificity may be attributed to the fact that Hg^{2+} has a much stronger affinity toward the amino and carboxylic groups on the CNPs surface than other metal ions.

To investigate the possibility of detection Hg^{2+} in living cells, we monitored the fluorescence spectra of CNP−RhB system in the presence of typical amino acids and RNA, as well as DNA. As shown in Figure 4b, except thiol-containing amino acids (Cys and Hcy), other types of biomolecules display negligible influence on the I_{437}/I_{575} ratio of the CNP−RhB nanohybrid

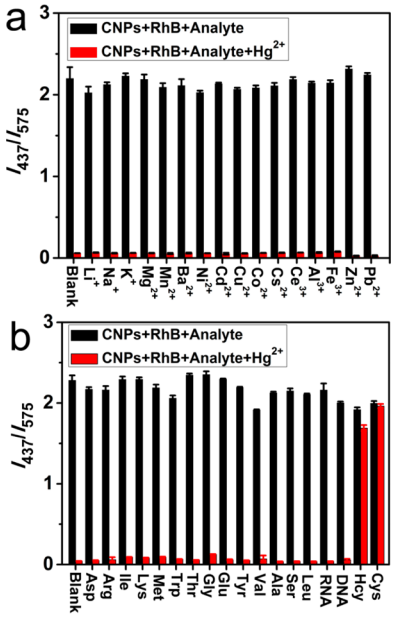

Figure 4. Selectivity of CNP−RhB nanohybrid system to Hg^{2+} in the presence of (a) other metal ions (25 μM) and (b) some amino acids (25 μM) or DNA, RNA in HEPES buffer solution (10 mM, pH 7.2). The black column and red column refer to the CNP−RhB nanohybrid solution in the absence and presence of 12 μM Hg^{2+}, respectively. Blank refers to free CNP−RhB nanohybrid solution. The error bars represent standard deviations based on three independent measurements.

system. The reason is that thiol functional groups have stronger binding ability to Hg^{2+} than CNPs. Overall, the results indicate that the present CNP−RhB nanohybrid has a high selectivity for Hg^{2+} against a wide variety of metal ions and the majority types of amino acids.

After we explored the CNP−RhB nanohybrid system's good selectivity and sensitivity for Hg^{2+} in HEPES buffer solution, we tested its application of sensing Hg^{2+} in lake water. It is expected that the water should contain many types of impurities that might interfere with the sensor. For the test, we collected lake water from a pond at the City University of Hong Kong, Hong Kong, China, and used it as a practical sample. The lake water sample was centrifuged at 6000 rpm for 20 min and then filtered through a 0.22 μm membrane. The absorption spectrum of the lake water sample is shown in Figure S7 (Supporting Information). A weak absorption band can be observed between 250 and 400 nm, which may be the absorbance of various impurities in the water. After mixing with CNPs and RhB, their characteristic absorption bands at about 350 and 554 nm are clearly observed.

The absorption and fluorescence titration spectra toward Hg^{2+} are shown in Figure 5. Addition of Hg^{2+} to the nanohybrid system results in a gradual blue shift of the absorption band between 250 and 400 nm, and decrease of PL intensity at 437 nm. Distinguishable fluorescence colors are also observed for the CNP−RhB nanohybrid solution (Figure 5b, inset). Apparently, these results indicate that the sensing can be qualitatively achieved by observing the color of the sensor under an UV irradiation through naked eyes without employing any analysis instrument. Again, the saturation of the I_{437}/I_{575} ratio occurs at $[Hg^{2+}]$ = 10 μM. Figure 5c shows the PL intensity ratio as a function of Hg^{2+} concentration. A good

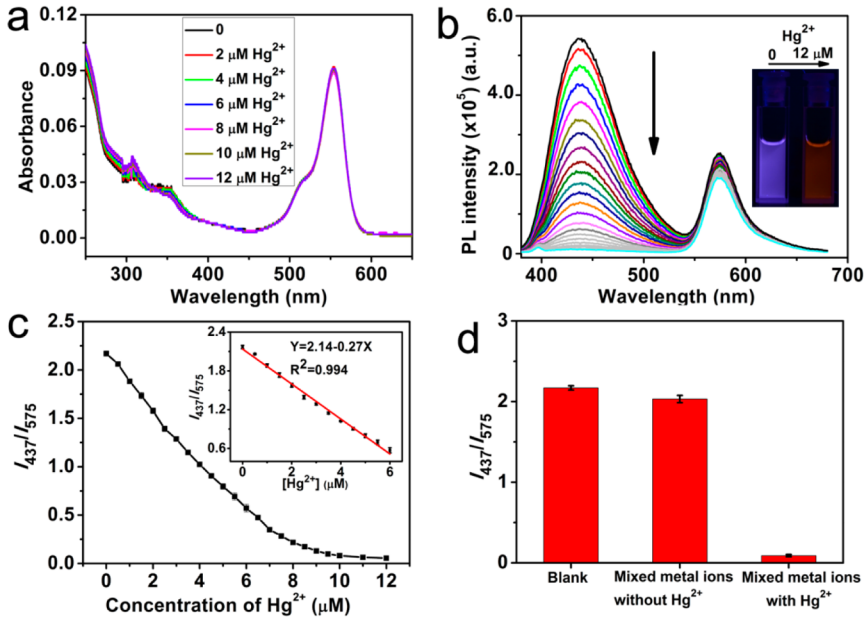

Figure 5. (a) Absorption and (b) fluorescence titration spectra of CNP−RhB nanohybrid in lake water upon gradual addition of Hg^{2+} from 0 to 12 μM. (λ_{ex} = 350 nm); (b, inset) photograph of CNP−RhB nanohybrid solution in the absence and presence of 12 μM Hg^{2+} under a UV light (365 nm). (c) Changes in the I_{437}/I_{575} ratio with incremental addition of Hg^{2+}; (inset) graph showing the linear relations between I_{437}/I_{575} and the concentrations of Hg^{2+}. (d) The difference in I_{437}/I_{575} ratio of CNP−RhB nanohybrid solution under various conditions in lake water. (Mixed metal ions including Li^+, Na^+, K^+, Mg^{2+}, Ba^{2+}, Mn^{2+}, Co^{2+}, Cu^{2+}, Cd^{2+}, Cs^{2+}, Ni^{2+}, Zn^{2+}, Pb^{2+}, Fe^{3+}, Al^{3+}, and Ce^{3+}; the concentration of each metal ions is 25 μM, and the concentration of Hg^{2+} is 12 μM).

linear relationship can be obtained in the concentration range of 0−6 μM. The limit detection is 45 nM.

The achievement of the high selectivity of an analyte of interest in a complex background of potentially competing species is a challenging task in sensor development. In this work, we also conducted the competition experiments in Hg^{2+} detection in the lake water containing other metal ions. Obvious I_{437}/I_{575} ratio diminishing of the CNP−RhB nanohybrid solution is observed upon the addition of Hg^{2+} regardless of the existence of competing species (Figure 5d). This reveals that the sensing of Hg^{2+} by the CNP−RhB nanohybrid is not influenced by other metal ions even in the samples randomly collected from our environment. These results suggest that the impurities in the real samples do not cause significant interferences to our sensor in the application of Hg^{2+} detection. Therefore, our sensor should be suitable for practical applications.

For further biological applications, MTT assays were carried out to evaluate the cytotoxicity of the CNPs and CNP−RhB nanohybrid system to A549 cells. As shown in Figure 6, with 24 h incubation, the cell viability of the A549 cells does not show obvious changes upon addition of CNPs of up to 1.0 mg/mL incubation. Even in the case of mixing with RhB, it still shows negligible cytotoxicity to A549 cells when the concentration is 0.5 mg/mL or below. Thus, the as-prepared CNP−RhB nanohybrid system can be used for cell imaging.

Figure 7 shows the bright field, fluorescence, and overlay images of living A549 cells incubated with CNP−RhB in the absence and presence of Hg^{2+}. After the cells are incubated with CNP−RhB for 4 h, strong blue and red fluorescence are observed inside the cells (Figure 7b,c). The overlay of blue and red channel fluorescence images shows violet color (Figure 7d). The sensing platform shows a good cell-permeability and maintains its dual-emission characteristic in the cellular environment. Then, the cellular Hg^{2+} sensing ability of

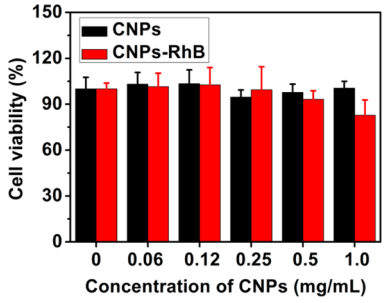

Figure 6. Cell viability values (%) estimated by MTT proliferation tests versus incubation concentration of CNPs and CNP−RhB for 24 h.

CNP−RhB nanohybrid system was further tested. In this context, a thiol-blocking reagent, *N*-ethylmaleimide (NEM), was first employed to react with the thiol-containing compounds in the cells; the cells were incubated with CNP−RhB nanohybrid solution, and then, 20 μM Hg^{2+} was added. No obvious blue fluorescence signal of the CNPs can be observed while the strong red fluorescence of RhB displays strong fluorescence (Figure 7f,g), implying that the cells uptake Hg^{2+}, and the ions completely quench the fluorescence of CNPs. This is in line with the change of the fluorescence spectrum observed in HEPES buffer solution. These results indicate that the CNP−RhB-based dual-emission nanohybrid system has great potential for imaging applications.

4. CONCLUSIONS

In summary, we have demonstrated that negatively charged and blue-emitting CNPs can form a nanohybrid system with a positively charged and red fluorescent organic dye through their electrostatic interaction. This CNP−RhB nanohybrid system is able to serve as a ratiometric fluorescence sensor for Hg^{2+}

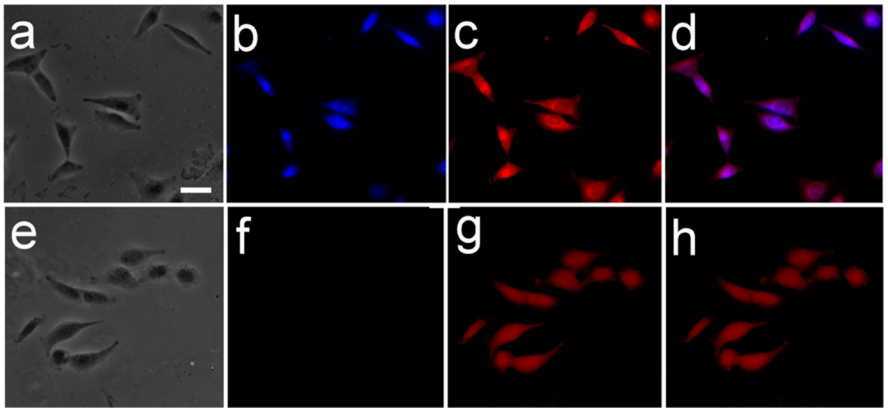

Figure 7. Images of A549 cells after being incubated with 200 μL of CNP−RhB nanohybrid solution in the (a−d) absence and (e−h) presence of Hg^{2+}; (a and e) bright-field images; (b and f) blue fluorescence field images; (c and g) red fluorescence field images; (d) the merge of images b and c; (h) the merge of images f and g. The scale bar is 20 μm.

detection with high selectivity and sensitivity in aqueous solution, environmental lake water, and living cells. The assay relies on the facts that the PL of the CNPs in the nanohybrid system is selectively quenched by Hg^{2+}, while the PL of RhB remains constant. Consequently, variation of the two PL intensities results in an obvious fluorescence color change from violet to orange upon the addition of Hg^{2+}, which can be easily observed by the naked eyes under UV light irradiation. The detection limit of such a sensor is as low as 42 nM.

Compared with previously reported sensing methods, our CNP−RhB nanohybrid system displays several important advantages. First, the assay is simple in design and offers a convenient "mix-and-detect" protocol for homogeneous and rapid detection of Hg^{2+} within 10 s in a wide pH range (pH 5−10). No subsequent chemical modification of CNPs is required after their preparation, offering a sensor with the advantages of simplicity, rapid response, and cost efficiency. Second, the CNP−RhB nanohybrid-based ratiometric fluorescence sensors can effectively eliminate the background interference and the fluctuation of detection conditions by built-in calibration of two emission peaks; the sensing process could be observed by naked eyes under a UV light, and therefore, the result is more reliable compared with single emission signal based sensors. Third, this novel strategy eliminates the need of employing semiconductor quantum dots and organic solvents, so it is much more environmental friendly. Fourth, this water-soluble sensing platform shows low cytotoxicity and good cell-permeability, and thus, it can be applied for intracellular sensing and imaging of Hg^{2+}. We expect that this strategy may offer a new approach for developing low-cost and sensitive dual-emission sensors for biological and environmental applications.

■ ASSOCIATED CONTENT

Supporting Information

XPS, FTIR, and zeta potential spectra; effect of pH or NaCl on the PL intensity at 437 nm of CNPs; absorption spectra of sole RhB or CNPs toward Hg^{2+}; and absorption spectrum of lake water sample. This material is available free of charge via the Internet at http://pubs.acs.org.

■ AUTHOR INFORMATION

Corresponding Authors

*Tel: +86-10-82543435. Fax: +86-10-82543435. E-mail: wangpf@mail.ipc.ac.cn.

*Tel: +(852)-34427433. Fax: +(852)-34420538. E-mail: apwjzh@cityu.edu.hk.

Author Contributions

The manuscript was written through contributions of all authors. All authors have given approval to the final version of the manuscript.

Notes

The authors declare no competing financial interest.

■ ACKNOWLEDGMENTS

This work was supported by the General Research Fund of Hong Kong (CityU 104911) and the National Natural Science Foundation of China (NSFC 51372213 and NSFC 61176007).

■ REFERENCES

(1) Renzoni, A.; Zino, F.; Franchi, E. Mercury Levels along the Food Chain and Risk for Exposed Populations. *Environ. Res.* **1998**, *77*, 68−72.

(2) Benoit, J. M.; Fitzgerald, W. F.; Damman, A. W. H. The Biogeochemistry of an Ombrotrophic Bog: Evaluation of Use as an Archive of Atmosphere Mercury Deposition. *Environ. Res.* **1998**, *78*, 118−133.

(3) Gutknecht, J. Inorganic Mercury (Hg^{2+}) Transport through Lipid Bilayer Membranes. *J. Membr. Biol.* **1981**, *61*, 61−66.

(4) Boening, D. W. Ecological Effects, Transport, and Fate of Mercury: A General Review. *Chemosphere* **2000**, *40*, 1335−1351.

(5) Tchounwou, P. B.; Ayensu, W. K.; Ninashvili, N.; Sutton, D. Environmental Exposure to Mercury and Its Toxicopathologic Implications for Public Health. *Environ. Toxicol.* **2003**, *18*, 149−175.

(6) Guo, T.; Baasner, J.; Gradl, M.; Kistner, A. Determination of Mercury in Saliva with a Flow-Injection System. *Anal. Chim. Acta* **1996**, *320*, 171−176.

(7) Wang, H. T.; Kang, B. S.; Chancellor, T. F., Jr.; Lele, T. P.; Tseng, Y.; Ren, F. Fast Electrical Detection of Hg(II) Ions with AlGaN/GaN High Electron Mobility Transistors. *Appl. Phys. Lett.* **2007**, *91*, 42114−42116.

(8) Leopold, K.; Foulkes, M.; Worsfold, P. Methods for the Determination and Speciation of Mercury in Natural Waters—A Review. *Anal. Chim. Acta* **2010**, *663*, 127−138.

(9) Bernaus, A.; Gaona, X.; Esbrí, J. M.; Higueras, P.; Falkenberg, G.; Valiente, M. Microprobe Techniques for Speciation Analysis and Geochemical Characterization of Mine Environments: The Mercury

District of Almadén in Spain. *Environ. Sci. Technol.* **2006**, *40*, 4090−4095.
(10) Senapati, T.; Senapati, D.; Singh, A. K.; Fan, Z.; Kanchanapally, R.; Ray, P. C. Highly Selective SERS Probe for Hg(II) Detection Using Tryptophan-Protected Popcorn Shaped Gold Nanoparticles. *Chem. Commun.* **2011**, *47*, 10326−10328.
(11) Chen, Y.; Wu, L. H.; Chen, Y. H.; Bi, N.; Zheng, X.; Qi, H. B.; Qin, M. H.; Liao, X.; Zhang, H. Q.; Tian, Y. Determination of Mercury(II) by Surface-Enhanced Raman Scattering Spectroscopy Based on Thiol-Functionalized Silver Nanoparticles. *Microchimica. Acta* **2012**, *177*, 341−348.
(12) Wu, J. S.; Liu, W. M.; Ge, J. C.; Zhang, H. Y.; Wang, P. F. New Sensing Mechanisms for Design of Fluorescent Chemosensors Emerging in Recent Years. *Chem. Soc. Rev.* **2011**, *40*, 3483−3495.
(13) Lan, M. H.; Wu, J. S.; Liu, W. M.; Zhang, W. J.; Ge, J. C.; Zhang, H. Y.; Sun, J. Y.; Zhao, W. W.; Wang, P. F. Copolythiophene-Derived Colorimetric and Fluorometric Sensor for Visually Supersensitive Determination of Lipopolysaccharide. *J. Am. Chem. Soc.* **2012**, *134*, 6685−6694.
(14) Lan, M. H.; Liu, W. M.; Wang, Y.; Ge, J. C.; Wu, J. S.; Zhang, H. Y.; Chen, J. H.; Zhang, W. J.; Wang, P. F. Copolythiophene-Derived Colorimetric and Fluorometric Sensor for Lysophosphatidic Acid Based on Multipoint Interactions. *ACS Appl. Mater. Interfaces* **2013**, *5*, 2283−2288.
(15) Miao, R.; Mu, L. X.; Zhang, H. Y.; She, G. W.; Zhou, B. J.; Xu, H. T.; Wang, P. F.; Shi, W. S. Silicon Nanowire-Based Fluorescent Nanosensor for Complexed Cu^{2+} and its Bioapplications. *Nano Lett.* **2014**, *14*, 3124−3129.
(16) Lee, M. H.; Kim, H. J.; Yoon, S.; Park, N.; Kim, J. S. Metal Ion Induced FRET OFF-ON in Tren/Dansyl-Appended Rhodamine. *Org. Lett.* **2008**, *10*, 213−216.
(17) Lee, M. H.; Van Giap, T.; Kim, S. H.; Lee, Y. H.; Kang, C.; Kim, J. S. A Novel Strategy to Selectively Detect Fe(III) in Aqueous Media Driven by Hydrolysis of a Rhodamine 6G Schiff Base. *Chem. Commun.* **2010**, *46*, 1407−1409.
(18) Lee, M. H.; Wu, J. S.; Lee, J. W.; Jung, J. H.; Kim, J. S. Highly Sensitive and Selective Chemosensor for Hg^{2+} Based on the Rhodamine Fluorophore. *Org. Lett.* **2007**, *9*, 2501−2504.
(19) Wu, J. S.; Hwang, I. C.; Kim, K. S.; Kim, J. S. Rhodamine-Based Hg^{2+}-Selective Chemodosimeter in Aqueous Solution: Fluorescent OFF-ON. *Org. Lett.* **2007**, *9*, 907−910.
(20) Liu, W. M.; Xu, L. W.; Zhang, H. Y.; You, J. J.; Zhang, X. L.; Sheng, R. L.; Li, H. P.; Wu, S. K.; Wang, P. F. Dithiolane Linked Thiorhodamine Dimer for Hg^{2+} Recognition in Living Cells. *Org. Biomol. Chem.* **2009**, *7*, 660−664.
(21) Gong, Y. J.; Zhang, X. B.; Chen, Z.; Yuan, Y.; Jin, Z.; Mei, L.; Zhang, J.; Tan, W. H.; Shen, G. L.; Yu, R. Q. An Efficient Rhodamine Thiospirolactam-Based Fluorescent Probe for Detection of Hg^{2+} in Aqueous Samples. *Analyst* **2012**, *137*, 932−938.
(22) Singh, A.; Raj, T.; Aree, T.; Singh, N. Fluorescent Organic Nanoparticles of Biginelli-Based Molecules: Recognition of Hg^{2+} and Cl^{-} in an Aqueous Medium. *Inorg. Chem.* **2013**, *52*, 13830−13832.
(23) Long, Y. F.; Jiang, D. L.; Zhu, X.; Wang, J. X.; Zhou, F. M. Trace Hg^{2+} Analysis via Quenching of the Fluorescence of a CdS-Encapsulated DNA Nanocomposite. *Anal. Chem.* **2009**, *81*, 2652−2657.
(24) Huang, D. W.; Niu, C. G.; Ruan, M.; Wang, X. Y.; Zeng, G. M.; Deng, C. H. Highly Sensitive Strategy for Hg^{2+} Detection in Environmental Water Samples Using Long Lifetime Fluorescence Quantum Dots and Gold Nanoparticles. *Environ. Sci. Technol.* **2013**, *47*, 4392−4398.
(25) Huang, D. W.; Niu, C. G.; Wang, X. Y.; Lv, X. X.; Zeng, G. M. "Turn-On" Fluorescent Sensor for Hg^{2+} Based on Single-Stranded DNA Functionalized Mn:CdS/ZnS Quantum Dots and Gold Nanoparticles by Time-Gated Mode. *Anal. Chem.* **2013**, *85*, 1164−1170.
(26) Baker, S. N.; Baker, G. A. Luminescent Carbon Nanodots: Emergent Nanolights. *Angew. Chem., Int. Ed.* **2010**, *49*, 6726−6744.
(27) Qu, S. N.; Wang, X. Y.; Lu, Q. P.; Liu, X. Y.; Wang, L. J. A Biocompatible Fluorescent Ink Based on Water-Soluble Luminescent Carbon Nanodots. *Angew. Chem., Int. Ed.* **2012**, *51*, 12215−12218.
(28) Wu, C. Y.; Wang, C.; Han, T.; Zhou, X. J.; Guo, S. W.; Zhang, J. Y. Insight into the Cellular Internalization and Cytotoxicity of Graphene Quantum Dots. *Adv. Healthcare Mater.* **2013**, *2*, 1613−1619.
(29) Ye, R. Q.; Xiang, C. S.; Lin, J.; Peng, Z. W.; Huang, K. W.; Yan, Z.; Cook, N. P.; Samuel, E. L. G.; Hwang, C. C.; Ruan, G. D.; Ceriotti, G.; Raji, A. R. O.; Marti, A. A.; Tour, J. M. Coal as an Abundant Source of Graphene Quantum Dots. *Nat. Commun.* **2013**, *4*, 2943−2948.
(30) Wang, Y. H.; Bao, L.; Liu, Z. H.; Pang, D. W. Aptamer Biosensor Based on Fluorescence Resonance Energy Transfer from Upconverting Phosphors to Carbon Nanoparticles for Thrombin Detection in Human Plasma. *Anal. Chem.* **2011**, *83*, 8130−8137.
(31) Xu, B. L.; Zhao, C. Q.; Wei, W. L.; Ren, J. S.; Miyoshi, D.; Sugimoto, N.; Qu, X. G. Aptamer Carbon Nanodot Sandwich Used for Fluorescent Detection of Protein. *Analyst* **2012**, *137*, 5483−5486.
(32) Ouyang, X. Y.; Liu, J. H.; Li, J. S.; Yang, R. H. A Carbon Nanoparticle-Based Low-Background Biosensing Platform for Sensitive and Label-Free Fluorescent Assay of DNA Methylation. *Chem. Commun.* **2012**, *48*, 88−90.
(33) Yu, C. M.; Li, X. Z.; Zeng, F.; Zheng, F. Y.; Wu, S. Z. Carbon-Dot-Based Ratiometric Fluorescent Sensor for Detecting Hydrogen Sulfide in Aqueous Media and inside Live Cells. *Chem. Commun.* **2013**, *49*, 403−405.
(34) Maiti, S.; Das, K.; Das, P. K. Label-Free Fluorimetric Detection of Histone Using Quaternized Carbon Dot-DNA Nanobiohybrid. *Chem. Commun.* **2013**, *49*, 8851−8853.
(35) Goncçalves, H.; Jorge, P. A. S.; Fernandes, J. R. A.; Esteves da Silva, J. C. G. Hg(II) Sensing Based on Functionalized Carbon Dots Obtained by Direct Laser Ablation. *Sens. Actuators, B* **2010**, *145*, 702−707.
(36) Zhou, L.; Lin, Y. H.; Huang, Z. Z.; Ren, J. S.; Qu, X. G. Carbon Nanodots as Fluorescence Probes for Rapid, Sensitive, and Label-Free Detection of Hg^{2+} and Biothiols in Complex Matrices. *Chem. Commun.* **2012**, *48*, 1147−1149.
(37) Lu, W. B.; Qin, X. Y.; Liu, S.; Chang, G. H.; Zhang, Y. W.; Luo, Y. L.; Asiri, A. M.; Al-Youbi, A. O.; Sun, X. P. Economical, Green Synthesis of Fluorescent Carbon Nanoparticles and Their Use as Probes for Sensitive and Selective Detection of Mercury(II) Ions. *Anal. Chem.* **2012**, *84*, 5351−5357.
(38) Yan, F. Y.; Zou, Y.; Wang, M.; Mu, X. L.; Yang, N.; Chen, L. Highly Photoluminescent Carbon Dots-Based Fluorescent Chemosensors for Sensitive and Selective Detection of Mercury Ions and Application of Imaging in Living Cells. *Sens. Actuators B* **2014**, *192*, 488−495.
(39) Dai, Q.; Liu, W. M.; Zhuang, X. Q.; Wu, J. S.; Zhang, H. Y.; Wang, P. F. Ratiometric Fluorescence Sensor Based on a Pyrene Derivative and Quantification Detection of Heparin in Aqueous Solution and Serum. *Anal. Chem.* **2011**, *83*, 6559−6564.
(40) Yang, C. J.; Jockusch, S.; Vicens, M.; Turro, N. J.; Tan, W. H. Light-Switching Excimer Probes for Rapid Protein Monitoring in Complex Biological Fluids. *Proc. Natl. Acad. Sci. U.S.A.* **2005**, *102*, 17278−17283.
(41) Han, Z. X.; Zhang, X. B.; Li, Z.; Gong, Y. J.; Wu, X. Y.; Jin, Z.; He, C. M.; Jian, L. X.; Zhang, J.; Shen, G. L.; Yu, R. Q. Efficient Fluorescence Resonance Energy Transfer-Based Ratiometric Fluorescent Cellular Imaging Probe for Zn^{2+} Using a Rhodamine Spirolactam as a Trigger. *Anal. Chem.* **2010**, *82*, 3108−3113.
(42) Cao, B. M.; Yuan, C.; Liu, B. H.; Jiang, C. L.; Guan, G. J.; Han, M. Y. Ratiometric Fluorescence Detection of Mercuric Ion Based on the Nanohybrid of Fluorescence Carbon Dots and Quantum Dots. *Anal. Chim. Acta* **2013**, *786*, 146−152.
(43) Lan, M. H.; Zhang, J. F.; Chui, Y. S.; Wang, H.; Yang, Q. D.; Zhu, X. Y.; Wei, H. X.; Liu, W. M.; Ge, J. C.; Wang, P. F.; Chen, X. F.; Lee, C. S.; Zhang, W. J. A Recyclable Carbon Nanoparticles-Based Fluorescent Probe for Highly Selective and Sensitive Detection of

Mercapto Biomolecules. *J. Mater. Chem. B* **2014**, DOI: 10.1039/C4TB01354A .

(44) Zheng, J.; Li, J. S.; Gao, X. X.; Jin, J. Y.; Wang, K. M.; Tan, W. H.; Yang, R. H. Modulating Molecular Level Space Proximity: A Simple and Efficient Strategy to Design Structured DNA Probes. *Anal. Chem.* **2010**, *82*, 3914−3921.

(45) Huang, J.; Zhu, Z.; Bamrungsap, S.; Zhu, G. Z.; You, M. X.; He, X. X.; Wang, K. M.; Tan, W. H. Competition-Mediated Pyrene-Switching Aptasensor: Probing Lysozyme in Human Serum with a Monomer-Excimer Fluorescence Switch. *Anal. Chem.* **2010**, *82*, 10158−10163.

(46) Kar, C.; Adhikari, M. D.; Ramesh, A.; Das, G. NIR- and FRET-Based Sensing of Cu^{2+} and S^{2-} in Physiological Conditions and in Live Cells. *Inorg. Chem.* **2013**, *52*, 743−752.

(47) Liu, R. H.; Li, H. T.; Kong, W. Q.; Liu, J.; Liu, Y.; Tong, C. Y.; Zhang, X.; Kang, Z. H. Ultra-Sensitive and Selective Hg^{2+} Detection based on Fluorescent Carbon Dots. *Mater. Res. Bull.* **2013**, *48*, 2529−2534.

(48) *National Primary Drinking Water Regulations*, EPA 816-F-09-004; U.S. Environmental Protection Agency: Washington, D.C., 2009.